China Ocean Eng., 2022, Vol. 36, No. 4, P. 629–637
DOI: https://doi.org/10.1007/s13344-022-0053-4, ISSN 0890-5487
http://www.chinaoceanengin.cn/ E-mail: coe@nhri.cn

Experimental Study on the Influence of Cross-Section Type of Marine Cable Conductors on the Bending Performance

YAN Jun[a, b], HU Hai-tao[a, b], LU Hai-long[a], YIN Yuan-chao[a], BU Yu-feng[a], LU Qing-zhen[b, c, *]

[a] State Key Laboratory of Structural Analysis for Industrial Equipment, Department of Engineering Mechanics, International Research Center for Computational Mechanics, Dalian University of Technology, Dalian 116024, China

[b] Ningbo Research Institute of Dalian University of Technology, Ningbo 315016, China

[c] State Key Laboratory of Structural Analysis for Industrial Equipment, School of Ocean Science and Technology, Dalian University of Technology, Panjin 124221, China

Received May 17, 2022; revised June 15, 2022; accepted July 18, 2022

Abstract

Through the development of marine energy, marine cables are the key equipment for transmission of electrical energy between surface platforms and underwater facilities. Fatigue failure is a critical failure mode of marine cables. The bending performance of the cable conductor has a major influence on both bending and fatigue performances of the overall cable structure. To study the influence of different types of the conductor cross-section on the bending performances of marine cable conductors, three types of copper conductors with the same cross-sectional area, i.e., noncompressed round, compressed round, and shaped wire conductors, were selected. The experimental results demonstrated that the cross-section type significantly affects the bending performances of copper conductors. In particular, the bending stiffness of the shaped wire conductor is the highest among the three conductor types. Four key evaluation parameters, i.e., the bending stiffness, maximum bending moment, envelope area, and engineering critical slip point, were selected to compare and analyze the bending hysteresis curves of the three copper conductors. The differences in the key evaluation parameters were analyzed based on the structural dimensional parameters, processing methods, and classical bending stiffness theoretical models of the three copper conductor types. The results provide an important theoretical guidance for the structural design and engineering applications of marine cable conductors.

Key words: marine cable conductors, cross-section type, bending performance, theoretical model, bending test

Citation: Yan, J., Hu, H. T., Lu, H. L., Yin, Y. C., Bu, Y. F., Lu, Q. Z., 2022. Experimental study on the influence of cross-section type of marine cable conductors on the bending performance. China Ocean Eng., 36(4): 629–637, doi: https://doi.org/10.1007/s13344-022-0053-4

1 Introduction

Owing to the rapid development of offshore oil and gas and wind power projects worldwide, marine cables such as submarine cables, umbilicals, and wind power cables are being increasingly used in marine energy development. Recently, the marine energy development has gradually moved toward deep water, and the power of the equipment used for marine energy development has increased. Moreover, the requirements for the structure and function of marine cables are constantly improving. Copper conductors are components that transmit electric energy in the marine cables, as shown in Fig. 1 (Wang et al., 2019). The common types of copper conductors, i.e., noncompressed round, compressed round, and shaped wire conductors, are shown in Fig. 2. Each of these conductor types is produced through different processing and manufacturing methods. In engineering applications, marine cable structures are subjected to ocean wave currents and floating body movements. Additionally, the cables are subjected to complex combined tensile and bending loads. In particular, reciprocating bending loads make cable structures (including copper conductors) prone to fatigue failure (Guo and Ye, 2020). Therefore, the marine cable structure must meet the flexibility and tensile strength requirements. Thus far, the marine cable structure adopts the form of a spiral winding, and therefore contact friction exists between the layers. Under a small bending curvature, the internal components of the structure can slide against each other, which improves the bending compliance of the structure. As the structure has a small spiral winding angle, it also exhibits a good tensile resistance. An accurate bending performance analysis for helically wound structures such as submarine cables, umbilicals, and marine risers

Foundation item: The work was financially supported by the National Natural Science Foundation of China (Grant No. U1906233), the Key R&D Program of Shandong Province (Grant No. 2019JZZY010801), the Development Projects in Key Areas of Guangdong Province (Grant No. 2020B1111040002), and the Fundamental Research Funds for the Central Universities (Grant Nos. DUT20ZD213 and DUT20LAB308).
*Corresponding author. E-mail: luqingzhen@dlut.edu.cn

applied in the offshore environment is important for the application of marine pipe and cable structures in the deep sea environment (Bai et al., 2015). Copper conductors are important structural and functional components of marine cables. Their structures also adopt the form of spiral winding. However, different sections of copper conductors lead to different forms of contact friction and bending moments of inertia, which affect the bending performances of copper conductors. The bending performance of a copper conductor is an important component of the overall bending performance of a marine cable structure. The selection of copper conductors with different cross-section types affects the bending performances of marine cable structures and fatigue life of marine cables in engineering applications, which ultimately affects the safety and reliability of marine cable structures. Therefore, it is important to study the influence of the cross-section type of copper conductors on their structural bending performance to ensure the structural safety of marine cables.

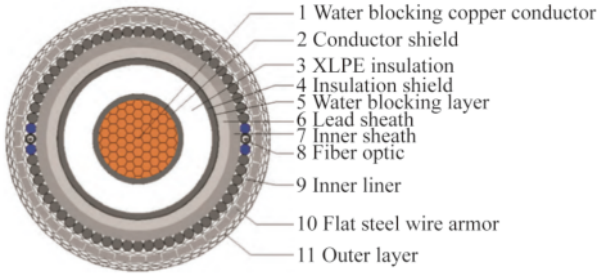

Fig. 1. Schematic of a typical marine cable structure (Wang et al., 2019).

The nonlinear bending performances of marine cables and marine flexible pipes with the same spiral winding structure characteristics have been extensively studied. Witz and Tan (1992) studied the nonlinear bending properties of marine cables, umbilicals, and flexible risers under bending load. They derived a calculation formula for the nonlinear bending stiffnesses of helically wound structures. They also demonstrated that, when the helically wound armored steel wire has a circular cross section, the impact of the torsional stiffness on the bending stiffness of the structure is negligible. This implies that the cross-section type of the helically wound steel wire influences the bending performance of the structure. Dong et al. (2015) considered the effects of tangential compliance and shear deformations on the layer bending behavior and proposed a new formula for calculation of the bending stiffness in the stick zone. Further, they derived a formula for the nonlinear bending stiffness of the helically wound structure in the slip transition zone with the variation of bending curvature, and concluded that the helically wound structure could never enter the full-slip zone. Tang et al. (2015) studied the bending nonlinear behaviors of marine flexible risers, where the armored wire in the riser was flat. Therefore, its bending stiffness calculation considered the moments of inertia in both directions of the flat wire. Additionally, they derived a theoretical formula based on the spring theory to calculate the bending stiffness in the case of a flat wire. Kraincanic and Kebadze (2001) proposed an analytical equation for prediction of the bending moment–curvature relationship of helically wound structures based on the Coulomb friction model and principle of virtual work. The bending stiffness was demonstrated to be a function of the bending curvature, friction coefficient between the layers, and contact pressure between them. Takahashi et al. (2020) focused on the influence of the boundary conditions at the contact between the armored steel wire and outer layer during the bending process. They established four theoretical models and performed bending performance tests with different forms of steel wire binding belts. Subsequently, the results of these tests were compared to those of the theoretical model. The forms of binding belts significantly influenced the bending behaviors of armored steel wires. Wang and Ji (2017) established an analytical model for the axisymmetric and bending analyses of an unbonded flexible riser. In this model, the interlayer contact pressure is considered, the sliding region is divided by the time step, and the bending stiffness of the next time step is determined. The bending moment–curvature relationship under an irregular response is discussed qualitatively. Zhang and Ostoja-Starzewski (2016) performed a finite-element simulation study on the nonlinear bending stiffness of cables. Moreover, they performed a sensitivity analysis to obtain the upper and lower values of bending stiffness considering the horizontal tension, friction coefficient, and contact type through the

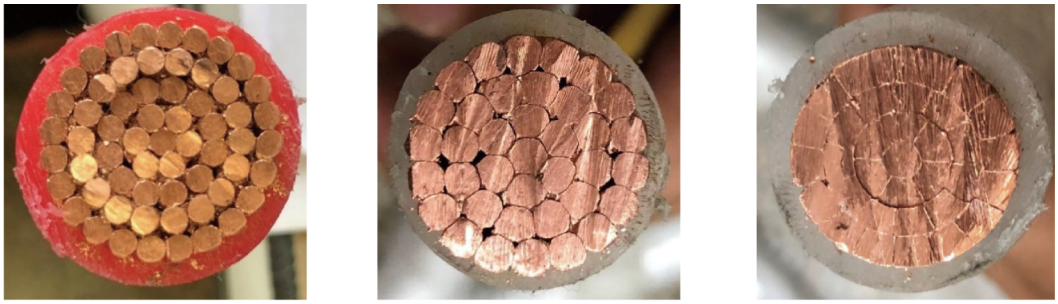

(a) Noncompressed round conductors (b) Compressed round conductors (c) Shaped wire conductors

Fig. 2. Common cross-section types of cable conductors.

simulation model. Chen et al. (2015) obtained a simplified evaluation method for calculation of the effective bending stiffness of a helically wound structure subjected to a quasi-static three-point bending test where they considered the influence of the end conditions and preload on the bending stiffness of this structure. Studies on the influence of the cross section of the helically wound copper conductor on its bending nonlinearity have not been reported. When the selection of copper conductor cross-section types was considered, some scholars (Hu et al., 2017; Yang et al., 2015; Zhang, 2018) only considered the economic factor of copper conductors and studied the influence of different cross-section types on processing and manufacturing costs.

Therefore, for the cable structure shown in Fig. 1, the choice of the cross-section type of the copper conductor is a key problem in the design of marine cable structures. It is necessary to study the bending nonlinearity performances of copper conductors with different cross-section types.

Accordingly, in this study, we investigated the nonlinear bending behaviors of noncompressed round, compressed round, and shaped wire conductors. In particular, using the three-point bending test method, reciprocating bending tests were performed for these three conductor types considering the same cross-sectional area. The key evaluation parameters of the conductor bending hysteresis curve were compared and analyzed, bending performance characteristics of the three copper conductor types were evaluated, and influencing factors of the key evaluation parameters were determined. The results of this study may serve as a useful reference for relevant structural design and engineering personnel.

2 Bending theoretical model of a helically wound structure

2.1 Nonlinear bending characteristics of a helically wound structure

Domestic and foreign scholars have conducted several studies on the bending performances of helically wound structures. It is generally considered that, under bending loads, helically wound structures exhibit nonlinear bending behaviors, being divided into three parts (Lu et al., 2013), as shown in Fig. 3. Segments OA, AB, and BC indicate the stick, slip transition, and full-slip zones, respectively. The curvatures corresponding to Points A and B represent the initial sliding curve κ_0 and curve κ_f, respectively. In engineering applications, the curvature corresponding to the tangent intersection of Segments OA and BC, i.e., Point D, is referred to as critical slip curvature κ_{cr}. When the helically wound structure is further bent by reducing the curvature after Point C, the bending moment–curvature relation is divided into other three stages: Segments CA', $A'B'$, and $B'C'$, which indicate the reverse stick, reverse slip transition, and reverse full-slip zones, respectively. The curvatures corresponding to Points A' and B' denote the reverse initial sliding curvature κ'_0 and reverse full sliding curvature κ'_f, respectively. The curvature corresponding to the tangent intersection of Segments CA' and $B'C'$, i.e., Point D', is defined as reverse critical slip curvature κ'_{cr}.

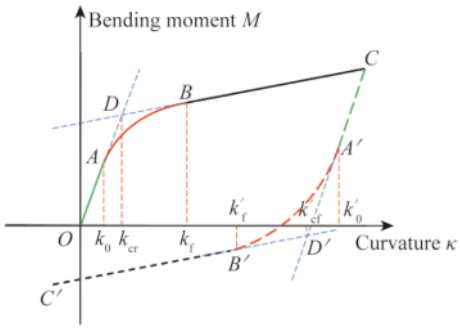

Fig. 3. Nonlinear bending behavior of a helically wound structure (Hu et al., 2022).

In the slip transition zone, as shown in Fig. 3, the bending stiffness changes gradually with the change in contact and friction, and cannot be expressed by the exact value. Moreover, in the stick and full-slip zones, the bending stiffness of the multilayer helically wound structure remains constant. Scholars have established different theoretical models that can be used to calculate its value in the two zones.

2.2 Introduction to the theoretical model of bending stiffness in the full-slip zone

As discussed above, the nonlinear bending behavior of the helically wound structure consists of three main stages in which its bending stiffness is generally considered linear in the stick and full-slip zones and nonlinear in the slip transition zone. Since the copper conductor with a multilayer helically wound structure is studied in this paper, the radius and angle of the helical copper wire in the inner layer of the copper conductor are very small. According to the equation in the literature, as follows Eq. (1), the value of $\kappa_{cr,t}$ of the copper conductor is also very small, so the copper conductor enters the slip transition zone at the beginning of the bending behavior. Therefore, the theoretical model in this paper only introduces the theoretical calculation model of bending stiffness in the full-slip zone.

$$\kappa_{cr,t} = \frac{2c_f q s_\alpha r R}{GJ\sin^2\alpha_i}, \tag{1}$$

where $\kappa_{cr,t}$ denotes the critical curvature for twisting slip. c_f, q, r, s_α, α_i, GJ, and R represent the internal friction coefficient, contact pressure at interface, radius of the wire, contact area of the wire arc, helix angle, helical strip's torsional stiffness, and radius of the helical strip, respectively.

When the bending of the structure enters the full-slip zone, the theoretical models available for the bending stiffness of the multilayer helically wound structure are as follows.

(1) Witz and Tan's theory

Witz and Tan (1992) derived a bending stiffness calculation equation for the full-slip zone in accordance with the

principle of energy conservation, which implies that, when a full slip occurs in a helically wound wire, the strain energy only considers the contribution of the bending and torsion of the armored steel wire section. When the spiral wire has a rectangular cross section,

$$K_{\mathrm{f}}^{\mathrm{W}}=\sum_{i=1}^{n}\frac{1}{2}\left(E_iI_n+E_iI_b\cos^2\alpha_i+GJ\sin^2\alpha_i\right), \tag{2}$$

while, when it is a round wire:

$$K_{\mathrm{f}}^{\mathrm{W}}=\sum_{i=1}^{n}\frac{1}{2}\left(E_iI_n+E_iI_b\cos^2\alpha_i\right), \tag{3}$$

where $K_{\mathrm{f}}^{\mathrm{W}}$ indicates the bending stiffness in the full-slip zone of the helically wound structure, as proposed by Witz and Tan (1992). E_i, I_n, and I_b represent the Young's modulus, principal moment of inertia, and secondary moment of inertia of the copper wire, respectively. The definitions of other physical quantities are the same as those in Eq. (1).

(2) Tang et al.'s theory

Tang et al. (2015) proposed a revised theoretical calculation model of bending stiffness in the full-slip zone and new calculation model based on the spring theory. The helical armor of the helically wound structure was regarded as a spring that could be freely bent. The radial deformation of the inner cylinder was ignored.

$$K_{\mathrm{f}}^{\mathrm{T}}=\sum_{i=1}^{n}\frac{2\cos\alpha_i}{\dfrac{1}{E_iI_n}+\dfrac{\cos^2\alpha_i}{E_iI_b}+\dfrac{\sin^2\alpha_i}{GJ}}, \tag{4}$$

where $K_{\mathrm{f}}^{\mathrm{T}}$ is the bending stiffness in the full-slip zone of the helically wound structure, as proposed by Tang et al. (2015). The definitions of other physical quantities are the same as those in Eqs. (1) and (2).

(3) Costello's theory

This theoretical model is mainly used for a helically wound steel wire with a round cross section. The equation for the bending stiffness in the full-slip zone is

$$K_{\mathrm{f}}^{\mathrm{C}}=\frac{\pi E}{4}\left[\frac{2n\cos\alpha_i}{\left(2+\nu\sin^2\alpha_i\right)}R_i^4+R_0^4\right], \tag{5}$$

where $K_{\mathrm{f}}^{\mathrm{C}}$ is the bending stiffness in the full-slip zone of the helically wound structure, as proposed by Costello (1997), R_0 is the radius of the central copper wire, ν is the Poisson's ratio of the material, and the definitions of other physical quantities are the same as those in Eq. (1). The spiral winding angle (α_i) in the reference (Costello, 1997) indicates the angle between the helical steel wire and transverse section of the cable. In this study, the spiral winding angle is uniformly defined as the angle between the spiral steel wire and axial section of the cable. To unify the angle in this study, the equation was transformed using a trigonometric function.

(4) Ramos et al.'s theory

Ramos Jr and Pesce (2004) considered the nonlinear behavior of the bending structure, which is attributed to the variation in the thickness of each layer and gap between the layers of the helically wound structure, and derived a theoretical equation for the bending stiffness of the full-slip zone:

$$K_{\mathrm{f}}^{\mathrm{R}}=\sum_{i=1}^{n}n_i\cos\alpha_i\left[GJ+\frac{3}{2}\left(E_iI_i-GJ\right)\cos^2\alpha_i\right], \tag{6}$$

where $K_{\mathrm{f}}^{\mathrm{R}}$ is the bending stiffness in the full-slip zone of the helically wound structure proposed by Ramos Jr and Pesce (2004), n is the number of spiral-wound layers, I_i is the inertia moment of the copper wire, and the definitions of other physical quantities are the same as those in Eqs. (1) and (2).

3 Bending test study on copper conductors

3.1 Bending test method

To study the influence of the cross-section type of the copper conductor on its bending performance, reciprocating bending tests on noncompressed round, compressed round, and shaped wire conductors were performed. Referring to the international test specifications, ISO(2009) and API (2014), we used a three-point bending method in this test to perform an experimental loading. A schematic of the experiment is shown in Fig. 4 (Hu et al., 2022). The experimental equipment includes a tensile and compression testing machine as a loading system and the load cell and displacement sensor frame as a data measurement equipment. The displacement and reaction force at the center of the copper conductor length were measured using displacement and force transducers, respectively, to study its three-point reciprocating bending mechanical behavior. The bending moment and curvature were calculated using Eqs. (7) and (8).

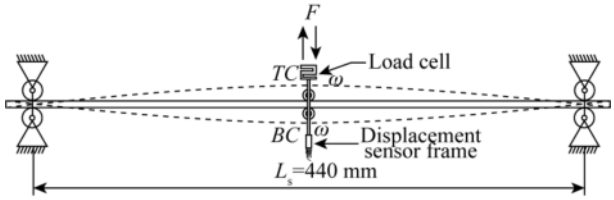

Fig. 4. Experimental setup of the reciprocating bending experiment of the copper conductor (Hu et al., 2022).

Both ends of the copper conductor were restrained by hinge supports. Its center was subjected to a vertical load to impose a reciprocating movement at that point. The length of the test piece between the two hinged supports was 440 mm. A displacement control was employed in the loading program. The upper and lower amplitudes of displacement loading were 6 mm, while the loading rate was 0.2 mm/s. The experiment was performed in the laboratory at the School of Marine Science and Technology, Dalian University of Technology.

The calculation formula for the bending moment is

$$M = FL_s/4. \tag{7}$$

The curvature calculation formula is

$$\frac{1}{\rho} = \frac{12\omega}{{L_s}^2}, \tag{8}$$

where $1/\rho$ is the curvature, F is the reaction force at the center of the copper conductor length, L_s is the copper conductor length between two hinge points, ω is the displacement applied to the copper conductor at its center, and M is the bending moment.

After the calculation of the bending moment M and curvature $1/\rho$ using the experimental data, $1/\rho$ was used as horizontal coordinate data, while M was used as vertical coordinate data to obtain the nonlinear bending curve of the copper conductor.

The cross-sectional dimensions of the three different types of copper conductors in Fig. 2 were measured. In this study, the filling coefficient of the compressed round conductors was 0.86. Owing to the small measurement errors and difficulty in measuring some of the data, we used the following assumptions, shown in Fig. 5. First, regarding the noncompressed round conductors, the copper wire in the conductor is a standard circle. Second, regarding the compressed round conductors, the randomness of the compressing process is negligible, and the cross section of the copper wire after compression is a standard hexagon. Third, regarding the shaped wire conductor, since there is no gap between the copper wires, for the convenience of calculation, it is assumed that the cross-section filling coefficient of the shaped wire conductors is 1. The height of each layer of the ladder type is the same and equal to the diameter of the copper wire at the center. The measurement of the internal spiral winding angle of the conductor was challenging. The internal spiral winding angle of the copper wire has a small effect on the bending mechanical properties of the conductor. Therefore, we assumed that each layer of the spiral copper wire in the conductor exhibited the same pitch.

After measurements, the following data on the cross sections of the three conductor types were obtained.

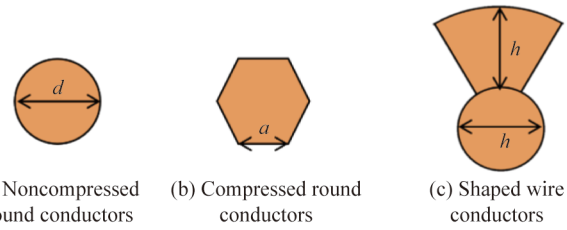

(a) Noncompressed round conductors (b) Compressed round conductors (c) Shaped wire conductors

Fig. 5. Simplified shapes of copper wires in conductors of different cross-section types.

In Table 1, the difference between the metal cross-sectional areas of the three copper conductor types is small; the maximum difference is 4.7%. Therefore, the three types of copper conductors were considered to have the same cross-sectional area. The filling coefficient of the shaped wire conductor was the largest, while that of the noncompressed round conductor was the smallest. The filling coefficient can provide a reference for studies on the mechanical properties of the three types of conductors. According to the cross-sectional shape and size of the copper wire in the conductor, the cross-sectional moment of inertia and area of the outermost copper wire of each cross-section conductor were calculated; the values are provided in Table 2.

3.2 Bending test results

The copper conductor specimen had an initial curvature at the beginning of the test. It was challenging to eliminate the influence of the initial curvature on the bending nonlinear performance at the beginning of the test loading. Therefore, in the data processing, to eliminate this influence from the experimental test results, the test result curve was shifted along the Y-axis so that the maximum values of the forward and reverse bending moments were equal. After the reciprocating bending test on the copper conductors, the third reciprocating bending test data were used as experimental results to reduce the test error. The experimental test results of the three different cross-section types of copper conductors are shown in Fig. 6.

Table 1 Dimensional data for marine cable conductors with three different cross-section types

Conductor type	Thickness of the sheath layer (mm)	Copper conductor diameter (mm)	Spiral angle of the outer copper wire (°)	Diameter of a single wire d (mm)	Side length of a regular hexagon a (mm)	Height of the ladder-type h (mm)	Metal cross-sectional area of copper conductors (mm^2)	Filling coefficient
Noncompressed round	1.5	21.5	15	2.35			264.58	0.73
Compressed round	1.5	19.5	13		1.63		256.84	0.86
Shaped wire	2.0	18.5	13			2.64	268.80	1

Table 2 Cross-sectional moment of inertia and area of the outermost copper wire of the three different cross-section types of conductors

Conductor type	Moment of inertia		Cross-sectional area of the outermost single copper wire (mm^2)
	Principal moments of inertia I_n (mm^4)	Secondary moment of inertia I_b (mm^4)	
Noncompressed round	1.50×10^{-12}	1.50×10^{-12}	4.34×10^{-6}
Compressed round	3.82×10^{-12}	3.82×10^{-12}	6.90×10^{-6}
Shaped wire	4.70×10^{-12}	6.78×10^{-12}	8.23×10^{-6}

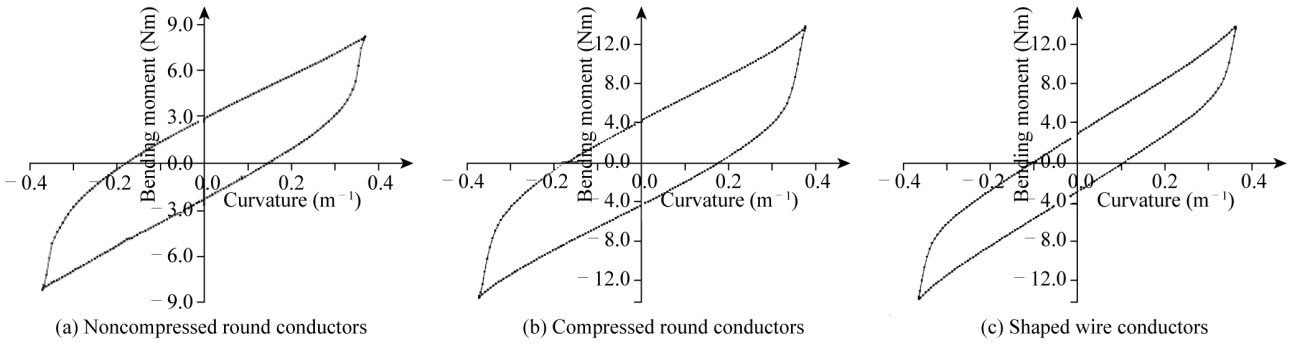

Fig. 6. Bending hysteresis curves of the three copper conductors with the different cross-section types.

4 Comparative analysis of experimental results

To facilitate the comparison of the experimental results for the three cross-section types of copper conductors, the experimental bending test results for the three cross-section types of copper conductors are plotted using the same coordinate system, as shown in Fig. 7.

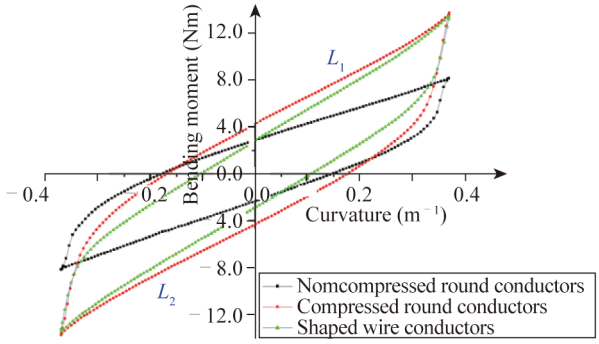

Fig. 7. Comparison of bending hysteresis experimental results of the three copper conductors with different cross-section types.

For the three different types of copper conductors subjected to reciprocating bending tests with the same maximum curvature, the plots of the bending moment during the bending process form a hysteresis curve owing to the interlayer contact friction.

4.1 Analysis of the fitted bending stiffness for the hysteresis curve

The multilayer helically wound copper conductor has a very small initial sliding curvature. It is challenging to measure its bending stiffness in the stick zone (Hu et al., 2022). Therefore, in this study, it was judged that the copper conductor entered the slip transition zone at the beginning of the test. To study the effect of different conductor cross-section types on the fitted bending stiffness of the hysteresis curve, a linear fitting was performed for each hysteresis curve using the full-slip section at two positions, labeled as L_1 and L_2 in Fig. 7, to obtain the fitted bending stiffness values. The results are presented in Table 3.

The data provided in Table 3 demonstrate that the bending stiffnesses obtained for the three copper conductor types were almost equal at L_1 and L_2, which indicates that the bending hysteresis curves obtained by the experimental tests were centrally symmetric and consistent with the characteristics of the bending hysteresis curves of helically wound structures. Thus, the results of the reciprocating bending experiments for the three types of cross-sectional copper conductors are reliable. The fitted bending stiffness was the largest and the smallest for the noncompressed round and shaped wire conductors, respectively, with a difference of 82.27% between these two values. This indicates that the conductor cross-section type demonstrated a larger influence on the bending stiffness of the conductor with the same cross-sectional area.

Based on the classical theoretical model presented in Section 2, the bending stiffness of the copper conductor at the full-slip section can be calculated using the material properties listed in Table 4. The average values of the fitting results at Positions L_1 and L_2, as provided in Table 3, were considered as experimental fitting results. The theoretical calculation and experimental fitting results were then compared and analyzed (Table 5).

The data provided in Table 5 indicate that, for the full-slip zone, four different theoretical models in Subsection 2.2 were used for the calculation. As the Costello's theoretical model only applies to round cross-sections of copper wire, it could not be applied to compressed round and shaped wire

Table 3 Fitted bending stiffnesses of copper conductors at different hysteresis curve positions

Conductor type	Bending stiffness			
	Bending stiffness at position L_1 (Nm²)	Difference (%)	Bending stiffness at position L_2 (Nm²)	Difference (%)
Noncompressed round	14.33		14.94	
Compressed round	22.80	59.11	22.57	51.07
Shaped wire	26.12	82.27	26.15	75.03

Table 4 Material parameters of the copper wire and outer sheath layer

	Poisson's ratio	Young's modulus (Pa)
Copper wire	0.30	1.18×10^{11}
Outer sheath layer	0.35	4.20×10^{8}

Table 5 Comparison of the theoretical and experimental results obtained for the bending stiffnesses of the copper conductors.

	Calculation method	Noncompressed round conductors		Compressed round conductors		Shaped wire conductors	
		Value (Nm^2)	Error (%)	Value (Nm^2)	Error (%)	Value (Nm^2)	Error (%)
Full-slip zone	Experimental results K_f	14.635		22.685		26.135	
	K_f^W	13.572	−7.26	18.919	−16.60	24.098	−7.79
	K_f^T	13.504	−7.73	18.623	−17.91	23.041	−11.84
	K_f^C	13.510	−7.69				
	K_f^R	14.616	−0.13	20.357	−10.26	26.023	−0.43

Note: The theoretical result K_f^R of the shaped wire conductor is the average calculation result of the primary and secondary moments of inertia of the trapezoidal copper wire.

conductors. As presented in Table 5, the calculated results of the theoretical model were consistent with the experimental fitting results of the full-slip zone. The results of the theoretical model were smaller than the experimental fitting results, because the theoretical model predicts the bending stiffness of the full-slip zone in the ideal state without considering the influence of the sheath layer extrusion pressure and contact friction on the bending stiffness of the copper conductor. The error between the theoretical and experimental results for the full-slip bending stiffness is the largest in the case of compressed round conductors, probably due to the processing residual stress and interlayer extrusion between the copper wires in the conductor during the compression process.

4.2 Analysis of the envelope area and maximum bending moment for the hysteresis curve

The envelope area of the hysteresis curve can be obtained by integrating the hysteresis curves of the different copper conductor types. These curves are shown in Fig. 7. The bending moment corresponding to each copper conductor at the maximum bending curvature was also extracted, and these values are listed in Table 6.

The data in Table 6 indicate that the envelope area formed by the compressed round conductor is largest, whereas the difference between the envelope area of the noncompressed round and shaped wire conductors is small. This indicates that the envelope area of the hysteresis curve significantly influenced by the interlayer extrusion pressure during processing. As the envelope area represents the energy loss during reciprocating bending, the compressed round conductor loses the highest amount of energy among the three copper conductor types during the reciprocating bending. Owing to this energy loss, the compressed round conductor suppresses the reciprocating bending and ocean vortex-induced vibrations in engineering applications.

Table 6 shows that the noncompressed round conductor has the smallest bending moment at the maximum curvature. Moreover, Table 3 shows that it had the smallest bending stiffness in the full-slip zone. The comparison of the cross-section types of the three conductors and cross-sectional moments of inertia of the outermost copper wire (Table 2) shows that the bending moments and cross-sectional bending stiffnesses of the different cross-section types of copper conductors under the same curvature are significantly affected by the moment of inertia of the cross section. A larger cross-sectional moment of inertia implies larger cross-sectional bending moment with the same curvature and bending stiffness in the full-slip section.

4.3 Comparative analysis of the engineering critical slip point for the hysteresis curve

As shown in Fig. 3, the intersection point of the tangent line, which is the engineering critical slip point, can be obtained by fitting the tangent line to the stick zone and full-slip zone of the bending nonlinear curve. As the stick zone was extremely short in this study, the experimental measurement of this zone was challenging. Therefore, in this study, to obtain the engineering critical slip point, an extremely small segment in reverse bending was used as the reverse stick zone and intersected with the tangent line of the reverse full-slip zone. By drawing the bending moment corresponding to the connection between the maximum bending moment and engineering critical slip curvature, the hysteresis curve can be simplified to the extent of consisting

Table 6 Comparison of hysteresis curve characteristics of cable conductors with different cross-section types

Conductor type	Maximum curvature (m^{-1})	Maximum bending moment (Nm)	Error (%)	Envelope area of hysteresis curve ($Nm\cdot m^{-1}$)	Error (%)
Noncompressed round	0.37	8.18		3.327	
Compressed round	0.37	13.78	68.46	5.571	67.45
Shaped wire	0.37	13.49	64.91	3.878	16.56

of four straight-line segments, as shown in Fig. 8, where the curvature difference from the reverse point to the engineering critical slip point is the slip curvature, while the bending moment difference is the slip bending moment. The relevant data information statistics are listed in Table 7.

The comparison of the simplified bending hysteresis curves of the three conductor types shows that the shaped wire conductor has the smallest slip curvature. It can be assumed that the shaped wire conductor first enters the full-slip zone. Considering the results in Table 2, the single copper wire of the shaped wire conductor has the largest cross-sectional area, which is consistent with the equation for critical slip curvature in the literature (Lu et al., 2020), where this curvature is proportional to the interlayer squeezing force and varies inversely with the cross-sectional area of the wire. The compressed round conductor has the largest slip curvature and largest slip moment. This indicates that the energy loss from the stick zone to the full-slip zone in the simplified hysteresis curve of the compressed round conductor is larger than those of the other two conductor cross-section types. Thus, the slip occurrence is less likely in this case. This phenomenon corresponds to the experimental results and explanations presented in Section 4.2.

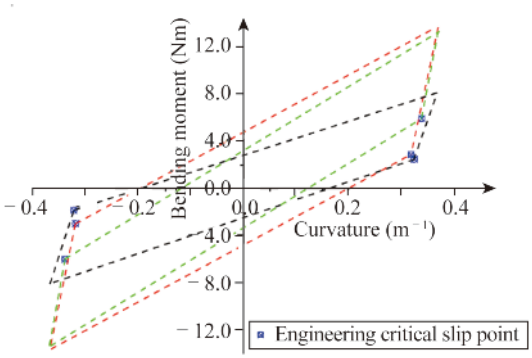

Fig. 8. Simplified bending hysteresis curve.

Table 7 Engineering critical slip point in hysteresis curves of copper conductors with different cross-section types

Conductor type	First quadrant			Third quadrant		
	Engineering critical slip point	Slip curvature (m^{-1})	Slip bending moment (Nm)	Engineering critical slip point	Slip curvature (m^{-1})	Slip bending moment (Nm)
Noncompressed round	(0.326, 2.499)	0.044	5.681	(−0.325, −1.872)	0.045	6.308
Compressed round	(0.320, 2.896)	0.050	10.884	(−0.322, −3.026)	0.048	10.754
Shaped wire	(0.340, 5.976)	0.030	7.514	(−0.342, −6.057)	0.028	7.433

5 Conclusions

In this study, reciprocating bending experiments were performed for three copper conductors with different cross sections. Through the experiments, we studied the changes in the bending performances of copper conductors with the same metal cross-sectional area but different cross-section types, and the key evaluation parameters in the bending hysteresis curves of copper conductors were compared and analyzed. The following conclusions were obtained.

(1) Copper conductors with the same metal cross-sectional area had different bending hysteresis curves owing to the different processing technologies and exhibited different bending stiffnesses of the full-slip zone. The section type of the copper conductor had a significant influence on its bending properties.

(2) In the reciprocating bending process, the energy dissipation of the compressed round conductor was the largest, which could restrain the reciprocating bending and vortex-induced vibrations in engineering applications.

(3) The bending performances of the copper conductors were strongly influenced by the moment of inertia and cross-sectional area of the copper wire and extrusion force between the layers. Among the considered cross-section types in this study, the shaped wire conductors were most prone to slippage during the bending because they exhibited the largest cross-sectional area for each copper wire.

References

API, 2014. *Recommended Practice for Flexible Pipe*, API RP 17B: 2014, American Petroleum Institute, Washington, DC.

Bai, X.L., Huang, W.P., Vaz, M.A., Yang, C.F. and Duan, M.L., 2015. Riser-soil interaction model effects on the dynamic behavior of a steel catenary riser, *Marine Structures*, 41, 53–76.

Chen, Z.H., Yu, Y.J., Wang, X.D., Wu, X.F. and Liu, H.B., 2015. Experimental research on bending performance of structural cable, *Construction and Building Materials*, 96, 279–288.

Costello, G.A., 1997. *Theory of Wire Rope*, Springer, New York.

Dong, L.L., Huang, Y., Dong, G.H., Zhang, Q. and Liu, G., 2015. Bending behavior modeling of unbonded flexible pipes considering tangential compliance of interlayer contact interfaces and shear deformations, *Marine Structures*, 42, 154–174.

Guo, Y. and Ye, N.Q., 2020. Numerical and experimental study on full-scale test of typical offshore dynamic power cable, *Proceedings of the 30th International Ocean and Polar Engineering Conference*, International Society of Offshore and Polar Engineers, Virtual.

Hu, G.H., Liu, C.W. and Fan, X.S., 2017. Cost comparison of non-compressed round and compressed round small-section conductor cables, *Optical Fiber & Electric Cable and Their Applications*, (3), 44–45. (in Chinese)

Hu, H.T., Yan, J., Sævik, S., Ye, N.Q., Lu, Q.Z. and Bu, Y.F., 2022. Nonlinear bending behavior of a multilayer copper conductor in a dynamic power cable, *Ocean Engineering*, 250, 110831.

ISO, 2009. *Petroleum and Natural Gas Industries - Design and Operation of Subsea Production Systems — Part 5: Subsea Umbilicals*, ISO 13628-5-2009, ISO.

Kraincanic, I. and Kebadze, E., 2001. Slip initiation and progression in helical armouring layers of unbonded flexible pipes and its effect on pipe bending behaviour, *The Journal of Strain Analysis for Engineering Design*, 36(3), 265–275.

Lu, H.L., Vaz, M.A. and Caire, M., 2020. A finite element model for unbonded flexible pipe under combined axisymmetric and bending loads, *Marine Structures*, 74, 102826.

Lu, Q.Z., Feng, L. and Yan, J., 2013. Time domain analysis of flexible risers considering non-linear bending stiffness, *Journal of Harbin Engineering University*, 34(11), 1352–1356. (in Chinese)

Ramos Jr, R. and Pesce, C.P., 2004. A consistent analytical model to predict the structural behavior of flexible risers subjected to combined loads, *Journal of Offshore Mechanics and Arctic Engineering*, 126(2), 141–146.

Takahashi, I., Masanobu, S., Kanada, S., Maeda, K., Manabe, H., Yamaguchi, T. and Tanaka, Y., 2020. Bending tests and cross-sectional analyses of multilayered flexible pipe models, *Journal of Marine Science and Technology*, 25(2), 397–410.

Tang, M.G., Yang, C., Yan, J. and Yue, Q.J., 2015. Validity and limitation of analytical models for the bending stress of a helical wire in unbonded flexible pipes, *Applied Ocean Research*, 50, 58–68.

Wang, K.P. and Ji, C.Y., 2017. Helical wire stress analysis of unbonded flexible riser under irregular response, *Journal of Marine Science and Application*, 16(2), 208–215.

Wang, W.C., Zhang, J.M., Zhao, Y.L., Chen, J., Ye, C. and Yan, Z.Y., 2019. Tension test and simulation analysis on flat-steel-wire-armoured optical fiber composite submarine cable, *High Voltage Engineering*, 45(11), 3467–3473. (in Chinese)

Witz, J.A. and Tan, Z., 1992. On the axial-torsional structural behaviour of flexible pipes, umbilicals and marine cables, *Marine Structures*, 5(2–3), 205–227.

Yang, S.H., Wang, W.D., Lin, F.T., Xu, Q.F., Pan, L. and Wang, Q., 2015. Comparison of the tile shaped and round conductor on structure and cost, *Electric Wire & Cable*, (6), 32–33, 44. (in Chinese)

Zhang, C., 2018. Optimization of cross-sectional area selection of control cable conductor in offshore platform, *Control and Instruments in Chemical Industry*, 45(9), 737–740. (in Chinese)

Zhang, D.S. and Ostoja-Starzewski, M., 2016. Finite element solutions to the bending stiffness of a single-layered helically wound cable with internal friction, *Journal of Applied Mechanics*, 83(3), 031003.